*Nano Research* 2017, 10(10): 3557–3570
DOI 10.1007/s12274-017-1567-6
Research Article

ISSN 1998-0124
CN 11-5974/O4

# Self-powered pressure sensor for ultra-wide range pressure detection

Kaushik Parida, Venkateswarlu Bhavanasi, Vipin Kumar, Ramaraju Bendi, and Pooi See Lee (✉)

*School of Materials Science and Engineering, Nanyang Technological University, Nanyang Avenue 639798, Singapore*

**Received:** 22 December 2016
**Revised:** 13 February 2017
**Accepted:** 2 March 2017



**KEYWORDS**
self-powered,
triboelectric,
piezoelectric,
nanogenerator,
pressure sensor

## ABSTRACT

The next generation of sensors should be self-powered, maintenance-free, precise, and have wide-ranging sensing abilities. Despite extensive research and development in the field of pressure sensors, the sensitivity of most pressure sensors declines significantly at higher pressures, such that they are not able to detect a wide range of pressures with a uniformly high sensitivity. In this work, we demonstrate a single-electrode triboelectric pressure sensor, which can detect a wide range of pressures from 0.05 to 600 kPa with a high degree of sensitivity across the entire range by utilizing the synergistic effects of the piezoelectric polarization and triboelectric surface charges of self-polarized polyvinyldifluoride-trifluoroethylene (P(VDF-TrFE)) sponge. Taking into account both this wide pressure range and the sensitivity, this device exhibits the best performance relative to that of previously reported self-powered pressure sensors. This achievement facilitates wide-range pressure detection for a broad spectrum of applications, ranging from simple human touch, sensor networks, smart robotics, and sports applications, thus paving the way forward for the realization of next-generation sensing devices. Moreover, this work addresses the critical issue of saturation pressure in triboelectric nanogenerators and provides insights into the role of the surface charge on a piezoelectric polymer when used in a triboelectric nanogenerator.

## 1 Introduction

Self-powered, interactive, maintenance-free, and multifunctional operation are the key requirements for the realization of next-generation electronics that could be applied to health monitoring, sensor networks, smart robotics, and sports applications [1–3]. One of the key components of any such next-generation electronics will be a pressure-monitoring system, capable of detecting a wide range of pressures with a high degree of sensitivity. There is an increasing need for materials and devices capable of precise and wide-range (ultra-low (<1 kPa), low (1–10 kPa), medium (10–100 kPa), and high (>100 kPa)) dynamic pressure detection for a spectrum of different applications, ranging from simple human touch to heavy object

Address correspondence to pslee@ntu.edu.sg

manipulation [4–5]. Extensive studies have been undertaken with the goal of fabricating precision pressure sensors, based on a range of mechanism types such as capacitive [6–8], resistive [9–11], piezoelectric [12–17], and triboelectric [18–23]. Resistive and capacitive-based pressure sensors exhibit high sensitivity and rapid response in the low- and medium-pressure ranges. However, most such pressure sensors are incapable of detecting a wide range of pressures with high sensitivity due to their inferior sensitivity at higher pressures [4, 7–9, 11]. Moreover, their operation is confined to static pressure monitoring, while they also require an external power source, such that they fall short of enabling the creation of a self-powered or maintenance-free pressure monitoring system. Piezoelectric and triboelectric pressure sensors are used for dynamic pressure sensing and self-powered sensing applications. Piezoelectric polymers have been the subject of extensive research for application to the fabrication of pressure sensors due to their high piezoelectric coefficient, structural flexibility, mechanical robustness, and low cost [12, 17, 24, 25]. A piezoelectric nanofiber-based pressure sensor was found to demonstrate an excellent low detection limit and a high sensitivity. However, the pressure detection range was small [17]. Additionally, piezoelectric polymers require time-consuming and complicated processing steps such as annealing (a thermal treatment to increase the crystallinity of the polymer) and electrical poling (the application of an electric field to align the dipoles) which increases the cost and constrains the integration of the polymer into different geometries and functional devices [26, 27]. Recently, the triboelectric nanogenerator (TENG), originally reported by Wang et al., has come to be regarded as a promising candidate for pressure-sensing applications due to its high sensitivity, low detection limit, and use in a wide variety of applications including tactile imaging, real-time tactile mapping, security surveillance, and healthcare monitoring [18, 22, 23]. However, the pressure detection range of the triboelectric pressure sensor is small, due to the saturation of the output voltage at higher pressures [21–23]. Thus, a major problem pertaining to all kinds of pressure sensors is their inability to sustain a high level of sensitivity over a wide range of pressures.

Herein, we introduce a novel self-polarized polyvinyldifluoride-trifluoroethylene (P(VDF-TrFE)) single-electrode triboelectric pressure sensor, capable of detecting a wide range of pressures with high sensitivity, by utilizing the synergistic effect of the piezoelectric polarization and triboelectric surface charges of a self-polarized P(VDF-TrFE) sponge. The single-electrode triboelectric pressure sensor (S-TEPS) can detect pressures ranging from 0.05 to 600 kPa with a high sensitivity of 0.104 $V{\cdot}kPa^{-1}$ (range = 0.05–5 kPa), 0.055 $V{\cdot}kPa^{-1}$ (range = 5–60 kPa) and 0.049 $V{\cdot}kPa^{-1}$ (range = 60–600 kPa). Most importantly, this work addresses the critical issue of saturation pressure (pressure at which the output voltage saturates in a triboelectric nanogenerator) and provides insights into the fundamental understanding of the role of surface charges in a piezoelectric polymer, when used as a triboelectric nanogenerator. Moreover, this work also addresses the persistent issue of poling porous piezoelectric polymers, by fabricating a self-poled porous P(VDF-TrFE) sponge using a modified breath-figure technique, which creates and aligns the piezoelectric β phase without the costly and tedious annealing and poling processes. The practical applicability of the S-TEPS device is demonstrated by utilizing the device in the human–machine interface, autonomous humanoid robots, and smart quadcopters.

## 2 Results and discussion

### 2.1 Self-poled porous P(VDF-TrFE) sponge

Figure 1(a) shows the highly flexible, rollable, and free-standing porous P(VDF-TrFE) sponge, fabricated by a modified breath-figure technique (as explained in the Experimental section). The film appears milky white due to the internal scattering of the light, caused by the pores present in the film [28]. The surface morphology of the film (Fig. 1(b)) clearly shows the porous structure (pore size ~10 μm). The pores are not only present on the surface but are distributed throughout the matrix of the film, which can be clearly seen in the cross-sectional field emission scanning electron microscope (FESEM) image (Fig. 1(c)). The inner pores present in the matrix of the film are much bigger than those on the surface. The presence of the

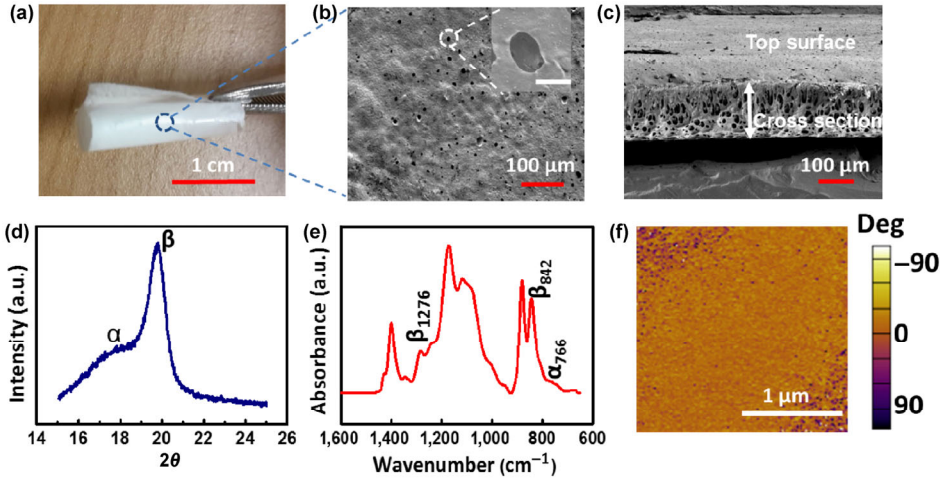


**Figure 1** (a) Self-poled porous P(VDF-TrFE) sponge. (b) FESEM image showing top view of self-poled porous P(VDF-TrFE) sponge. Inset in (b) is an enlarged FESEM image showing a pore. Scale bar: 10 μm. (c) Cross-sectional FESEM images of self-poled porous P(VDF-TrFE) sponge. (d) XRD spectra of self-poled porous P(VDF-TrFE) sponge. (e) FTIR spectra of self-poled porous P(VDF-TrFE) sponge. (f) PFM phase image of the self-poled porous P(VDF-TrFE) sponge.

pores makes the film spongy and compressible. The piezoelectric behavior of the P(VDF-TrFE) sponge is due to the presence of the β phase, which was confirmed by X-ray diffraction (XRD) and Fourier transform infrared spectroscopy (FTIR). Figure 1(d) shows the XRD pattern for the porous P(VDF-TrFE) sponge. The predominant peak at $2\theta$ = 19.7° corresponds to the (110)/(200) planes of the piezoelectric β phase [29, 30]. Minor amounts of α phase can be found with the shoulder peak at $2\theta$ = 18°. The FTIR spectroscopy analysis of the P(VDF-TrFE) sponge further validates the presence of the β phase. Figure 1(e) illustrates the absorption infrared spectra of the P(VDF-TrFE) porous sponge. The absorption bands at 842 and 1,276 $cm^{-1}$ are characteristic traits of the piezoelectric β phase [12, 31].

The self-polarization phenomenon of the P(VDF-TrFE) sponge was analyzed using piezo-response force microscopy (PFM). The observed uniform contrast in the phase behavior of the porous P(VDF-TrFE) sponge (Fig. 1(f)), reveals the unipolar orientation of the dipoles. For comparison, a PFM analysis of the control sample (non-poled compact P(VDF-TrFE) film prepared by a spin-coating method with similar dimensions) was carried out as shown in Fig. S1(a) in the Electronic Supplementary Material (ESM). The domains with different orientations in Fig. S1(a) (in the ESM) exhibit the randomly oriented dipoles of the non-poled compact P(VDF-TrFE) film [32]. The self-alignment of the dipoles in the porous P(VDF-TrFE) sponge indicates the promising potential of the energy-harvesting behavior of the piezoelectric film [26, 33], which was investigated by measuring the voltage output upon the application of mechanical pressure. Figure 2(a) is a schematic of a self-poled porous P(VDF-TrFE) piezoelectric nanogenerator (PENG). When a pressure of 625 kPa (a force of 62.5 N exerted on an area of 1 $cm^2$) at a frequency of 20 Hz was exerted on the self-poled P(VDF-TrFE) PENG, an output voltage of 21 V (Fig. 2(b)) and a current density of 2.25 $\mu A \cdot cm^{-2}$ (Fig. 2(c)) was generated. The mechanical pressure reorients the aligned molecular dipoles, causing a change in the polarization or the dipole density of the self-poled P(VDF-TrFE) sponge; this creates an internal piezoelectric potential. The free charge carriers (present at the metal electrodes) flow from the higher potential region to the lower potential region through the external connections to balance the internal piezoelectric potential, thus giving rise to a positive peak. When the pressure is released, the change in the polarization diminishes, and hence the internal piezoelectric potential falls to zero, such that the free-charge carriers return across the external circuit, giving rise to a negative peak [31, 34]. The difference in strain rates during force application and release leads to the difference in the magnitudes of the positive and

negative peaks, which is similar to the findings of other works on piezoelectric nanogenerators [35, 36]. The power density ($P = VI$) of the self-poled porous P(VDF-TrFE) sponge, measured at the same pressure and frequency, was 47.25 μW·cm$^{-2}$. The control sample (non-poled compact P(VDF-TrFE) spin-coated film with a similar thickness and working area), generates an output voltage of 0.6 V, at the same pressure and frequency (Fig. S1(b) in the ESM). This indicates that the self-poled porous P(VDF-TrFE) sponge has a superior piezoelectric energy-harvesting performance, with the output voltage being enhanced by a factor of 35, compared with that of the control sample when measured under similar conditions. The enhancement of the output voltage can be attributed to the effective self-polarization of the P(VDF-TrFE) sponge, without any annealing or external poling processes. Further, the energy-harvesting performance of the poled compact P(VDF-TrFE) (with similar dimensions) was measured under similar conditions. The poled compact P(VDF-TrFE) PENG (poled with an electric field of 20 V·μm$^{-1}$ at 100 ℃) generates a voltage of 5 V and an average current density of 0.7 μA·cm$^{-2}$ (Fig. S2 in the ESM). The output voltage produced by the self-poled porous P(VDF-TrFE) PENG increased by a factor of 4, relative to the compact film, due to its porous structure. The porous structure increases the compressibility but decreases the dielectric constant which, in turn, increases the output voltage [37].

The self-polarization behavior of the porous P(VDF-TrFE) sponge can be attributed to the modified breath-figure technique adopted to fabricate the P(VDF-TrFE) sponge. Usually, the breath-figure technique (also known as the vapor-induced phase-separation technique) is used to create porous polymers by exposing a drop-cast or spin-coated polymer solution to humidity at room temperature (25 ℃) [28, 38, 39]. In the presence of humidity, water vapor condenses onto the solution. This acts as a mold for the pores and the polymer nucleates around the water droplets. In our modified breath-figure technique, the drop-cast polymer solution was exposed to humidity (50% relative humidity (RH)) at a temperature of −20 ℃. Self-polarized porous P(VDF-TrFE) sponge was obtained using the modified breath-figure technique. However, the film prepared using the typical breath-figure technique (at room temperature, 25 ℃), fails to exhibit alignment of the P(VDF-TrFE) molecular dipoles (as indicated by the piezoelectric energy-harvesting performance shown in Fig. S3(a) in the ESM). The self-polarization effect was observed only when the breath-figure technique was performed at a temperature below 0 ℃ (as indicated by the piezoelectric energy-harvesting performance measured with the variation in the fabrication temperature, indicated by Fig. S3(b) in the ESM). Moreover, it was observed that a film fabricated at a temperature of −20 ℃ in the absence of humidity (<5% RH), fails to exhibit alignment of the P(VDF-TrFE) dipoles (as indicated by the piezoelectric energy-harvesting performance, shown in Fig. S4 in the ESM). Therefore, self-polarization was actualized when the temperature was low (below 0 ℃) and humidity was present. P(VDF-TrFE) consists of a repetitive unit block of $CH_2CF_2$; the electro-negative fluorine and the electro-positive hydrogen attached to the carbon backbone act as a molecular dipole. The electro-negative fluorine forms a hydrogen bond (H-bond) with the O–H group of the water molecules, as verified by the presence of a peak at the 3,600–3,120 cm$^{-1}$ region of the FTIR spectrum (Fig. S5 in the

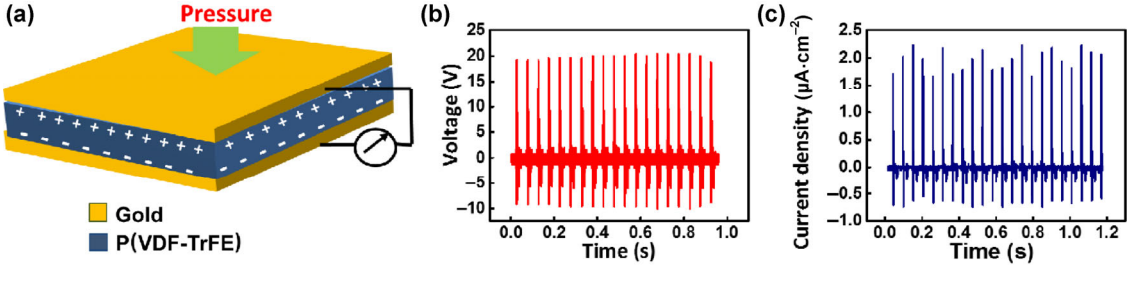


**Figure 2** (a) Schematic diagram of self-poled porous P(VDF-TrFE) piezoelectric nanogenerator (PENG). (b)Voltage output of self-poled porous P(VDF-TrFE) PENG subjected to a pressure of 625 kPa exerted at a frequency of 20 Hz. (c) Current density of self-poled porous P(VDF-TrFE) PENG subjected to a pressure of 625 kPa exerted at a frequency of 20 Hz.

ESM) [40–42]. H-bonding has been widely regarded as causing self-alignment in PVDF, as reported for PVDF-AlO-rGO composite films [41], PVDF-cerium composite films [43], and Langmuir–Blodgett deposited PVDF films [42]. However, for films prepared by the typical breath-figure technique (at 25 ℃ and 50% RH), the interactions of the water molecules (trapped inside the polymer solution) with P(VDF-TrFE) molecular dipoles are not stable, as the thermal energy (at room temperature, 25 ℃) is sufficient to create random motion of the water molecules, such that the dipoles fail to align during the nucleation of the P(VDF-TrFE) film. With our modified breath-figure technique (below 0 ℃ and 50% RH), water vapor condenses onto the P(VDF-TrFE) solution and forms solid ice crystals, around which the P(VDF-TrFE) nucleates. The solid ice crystals exhibit stable interactions with the P(VDF-TrFE) dipoles, which freeze the aligned dipoles (caused by the H-bonding interaction) during the nucleation process. Subsequently, when the water was evaporated from the P(VDF-TrFE) film (by drying at room temperature), a porous self-polarized P(VDF-TrFE) sponge was obtained. The self-polarization observed for the porous P(VDF-TrFE) film, fabricated by our modified breath-figure technique, can be attributed to the stable H-bonding interaction between the solid ice (water) crystal molecular dipoles and the PVDF molecules which align the P(VDF-TrFE) dipoles at low temperatures (<0 ℃). However, a detailed understanding of the role of H-bonding in self-alignment is not clear at this stage, such that further investigation will be necessary. To the best of our knowledge, this is the first report on a self-polarized porous piezoelectric polymer, and the results of this study expand our know-how related to the fabricating of self-polarized compact films [42], composite films [41, 43], and nanowire-based [33] piezoelectric polymers. In addition, this solves the difficulty of poling porous piezoelectric materials, which often leads to dielectric breakdown [44]. The modified breath-figure technique provides a simple, scalable, and cost-effective alternative to currently available piezoelectric polymer processing techniques, thus creating a disruptive technology for preparing piezoelectric energy harvesters and sensor devices.

### 2.2 Self-powered single-electrode triboelectric pressure sensor

#### *2.2.1 Mechanism of single-electrode triboelectric pressure sensor*

Figure S6(a) in the ESM is a schematic illustration of a single-electrode triboelectric pressure sensor (S-TEPS). The device consists of Au/P(VDF-TrFE) and polydimethylsiloxane (PDMS) film, separated by a spacer. The self-poled P(VDF-TrFE) (negatively polarized surface, Fig. S7(a) in the ESM) was used as the triboelectric positive material, and PDMS was used as the triboelectric negative material in the S-TEPS. Figure 3(a) is a schematic depiction of the complete process of mechanical pressure application and release for a self-poled P(VDF-TrFE) S-TEPS. The mechanism of the triboelectric pressure sensor is based on the coupling between the triboelectric and electrostatic induction effects [45–48]. Before the application of mechanical force, the self-poled P(VDF-TrFE) film and the PDMS were not in contact; hence there are no surface charges on the films. Upon the application of mechanical pressure, the self-poled P(VDF-TrFE) sponge comes into contact with the PDMS. Upon making contact, the surface of the self-poled P(VDF-TrFE) acquires a positive charge while the surface of the PDMS acquires a negative charge due to the differences in their triboelectric polarities [45, 49]. When the mechanical pressure is released, an air gap is formed between the two oppositely charged surfaces (PDMS and self-poled P(VDF-TrFE) sponge), thus creating an electrical potential difference between the metal contact and the ground. This potential difference results in a transient flow of charge. When the compressive force is reapplied, the separation between the two oppositely charged surfaces is reduced. Thus, the electrical potential difference decreases, resulting in the charge flowing in the opposite direction [50–52].

#### *2.2.2 Non-poled P(VDF-TrFE) single-electrode triboelectric pressure sensor*

For comparison, the pressure-sensing performance of the non-poled P(VDF-TrFE) sponge (prepared using a typical breath-figure technique, at 25 ℃ and 50% RH) was first analyzed, using the device configuration

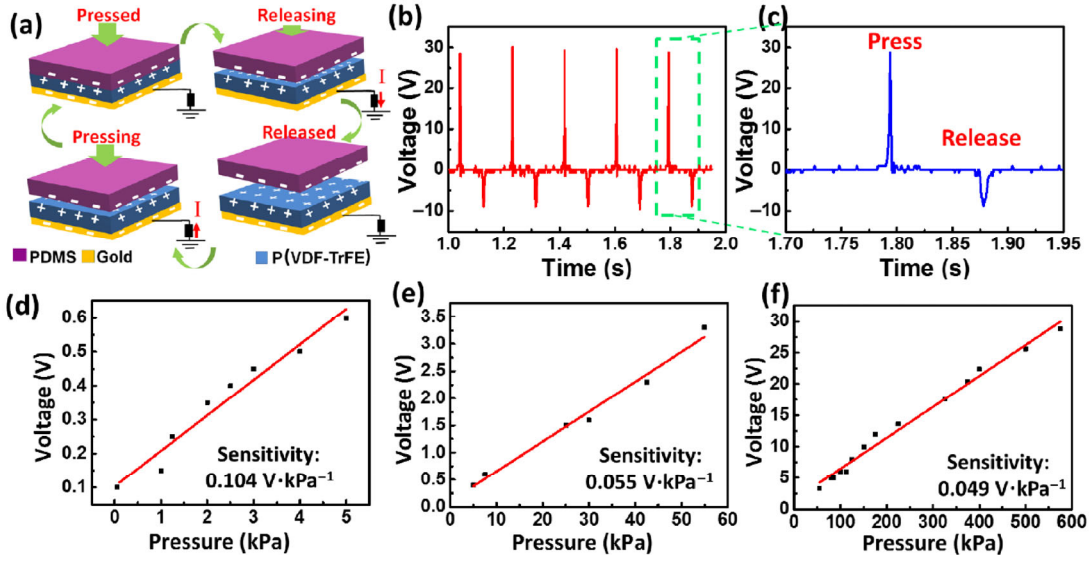


**Figure 3** (a) Overall process of mechanical pressure application and release for P(VDF-TrFE) S-TEPS. (b) Voltage output of self-poled P(VDF-TrFE) S-TEPS subjected to a pressure of 600 kPa exerted at a frequency of 5 Hz. (c) Voltage output pulse of self-poled P(VDF-TrFE) S-TEPS when pressed and released. (d) Voltage output of self-poled P(VDF-TrFE) S-TEPS for low-pressure range (0.05 to 5 kPa). (e) Voltage output of self-poled P(VDF-TrFE) S-TEPS for medium-pressure range (5 to 60 kPa). (f) Voltage output of self-poled P(VDF-TrFE) S-TEPS for high-pressure range (60 to 600 kPa).

shown in Fig. S6 in the ESM. Figure S8(a) in the ESM shows the voltage output response of the non-poled P(VDF-TrFE) S-TEPS at a mechanical pressure of 600 kPa (a force of 60 N exerted on an area of 1 $cm^2$) applied at a frequency of 5 Hz. For low (0.05–5 kPa) and medium (5–50 kPa) pressures (Figs. S8(b) and S8(c) in the ESM), the non-poled P(VDF-TrFE) S-TEPS exhibits a linear increase in the output voltage with an increase in the dynamic pressure (exerted at a frequency of 5 Hz). The sensitivities of the non-poled P(VDF-TrFE) S-TEPS for the low- and medium-pressure ranges are 0.089 and 0.053 $V{\cdot}kPa^{-1}$, respectively. The sensitivity was calculated from the voltage response slope (Figs. S8(b) and S8(c) in the ESM) [17, 21]. This device exhibits good sensitivity in the lower- and medium-pressure ranges. However, as the pressure was increased beyond 50 kPa, the output voltage was found to saturate (Fig. S8(d) in the ESM), and thus the sensitivity (0.0002 $V{\cdot}kPa^{-1}$) of the non-poled P(VDF-TrFE) S-TEPS degrades, the same as that reported in other works on triboelectric nanogenerators [21–23].

The output voltage generated by a triboelectric nanogenerator depends on the surface charge density, which in turn is affected by the interfacial contact area between the two polymers [52]. With a gradual increase in the mechanical pressure, the interfacial contact area increases due to macroscopic deformation at the interface between the two polymers. At a certain saturation pressure, the two polymers are in complete contact with each other, thus saturating the triboelectrically induced surface charge, which restrains any further increase in the output voltage. The saturation pressure depends on the polymer material and the interfacial surface area [53]. The saturation pressure (usually around 5 to 100 kPa for TENG) often limits the operation of TENG as a wide-range pressure sensor [18]. This problem can be circumvented by using our self-polarized P(VDF-TrFE) sponge (described below), which extends the limits of the saturation pressure.

### 2.2.3 *Self-poled P(VDF-TrFE) single-electrode triboelectric pressure sensor*

The pressure-sensing performance of the self-poled P(VDF-TrFE) sponge was evaluated using the device configuration shown in Fig. S6(a) in the ESM. Figure S6(b) shows the self-poled P(VDF-TrFE) S-TEPS. When mechanical pressure is exerted on the self-poled P(VDF-TrFE) S-TEPS, two phenomena occur simultaneously. One is the generation of a triboelectrically

induced surface charge on the self-poled P(VDF-TrFE) sponge which is due to contact-separation between the self-poled P(VDF-TrFE) sponge and the PDMS film. Second is the generation of polarization-induced surface charges on the self-poled P(VDF-TrEF) sponge due to the internal piezoelectric potential difference across the P(VDF-TrEF) sponge (caused by the reorientation of the aligned molecular dipoles under mechanical stress) [54]. These two different phenomena are factors governing the total output voltage generated by the self-poled P(VDF-TrFE) S-TEPS upon the application of mechanical pressure. For the triboelectrically induced surface charges, a voltage is generated when the two polymers (self-poled P(VDF-TrFE) sponge and PDMS film) approach and separate from each other. For the polarization-induced surface charges, a voltage is generated when the two polymers are in contact (causing an internal piezoelectric potential difference under mechanical stress).

Figures 3(b) and 3(c) shows the voltage output response of the self-poled P(VDF-TrFE) S-TEPS at a mechanical pressure of 600 kPa (a force of 60 N exerted over an area of 1 $cm^2$) with a frequency of 5 Hz. For the low- (0.05–5 kPa, Fig. 3(d)) and medium- (5–50 kPa, Fig. 3(e)) pressure ranges, the self-poled P(VDF-TrFE) sponge shows a sensitivity of 0.104 $V{\cdot}kPa^{-1}$ and 0.055 $V{\cdot}kPa^{-1}$, respectively (for a dynamic mechanical pressure exerted at a frequency of 5 Hz). However, the sensitivities of the self-poled P(VDF-TrFE) S-TEPS for the low- and medium-pressure ranges are comparable with those of the non-poled P(VDF-TrFE) S-TEPS (Figs. S8(b) and S8(c) in the ESM). This reveals that the polarization-induced surface charge does not significantly affect the performance of the self-poled P(VDF-TrFE) S-TEPS at the lower- and medium-pressure ranges. In the lower- and medium-pressure ranges, the piezoelectric potential generated across the self-poled P(VDF-TrFE) sponge is very low (as shown in the piezoelectric energy-harvesting performance of the self-poled P(VDF-TrFE) sponge, measured at a frequency of 5 Hz, (Fig. S9 in the ESM)), thus inducing less polarization-induced surface charge on the self-poled P(VDF-TrFE) sponge. Hence, in the low-and medium-pressure ranges, the triboelectically induced surface charge dominates.

However, in the high-pressure range (50 to 600 kPa, Fig. 3(f)), the self-poled P(VDF-TrFE) S-TEPS demonstrates a sensitivity of 0.049 $V{\cdot}kPa^{-1}$, which is 245 times greater than that of the non-poled P(VDF-TrFE) S-TEPS. Beyond 50 kPa, the triboelectrically induced surface charge saturates, as the PDMS film and self-poled P(VDF-TrFE) sponge are completely in contact with each other (as indicated for the non-poled P(VDF-TrFE) S-TEPS, (Fig. S8(d) in the ESM)). Notably, beyond 50 kPa, the piezoelectrically induced surface charge increases due to the increment of the internal piezoelectric potential with the increase in the mechanical pressure. Beyond the saturation pressure (50 kPa), the polarization-induced surface charge dominates, such that the output voltage continues to increase, while the triboelectrically induced surface charge is saturated. Thus, the self-poled P(VDF-TrFE) S-TEPS can detect a wide range of pressures from 0.05 to 600 kPa without any loss of sensitivity. To the best of our knowledge, taking into account both the wide pressure-sensing range and the sensitivity, the self-poled P(VDF-TrFE) S-TEPS offers the best performance of all the self-powered pressure sensors reported to date (Table S1 in the ESM).

The charge transfer for the self-poled P(VDF-TrFE) S-TEPS (voltage output generated due to the piezoelectric polarization and triboelectric effect, Fig. 4(a)) is 4.3 times greater than the non-poled P(VDF-TrFE) S-TEPS (voltage output generated due to only the triboelectric effect, Fig. S10 in the ESM). This validates the higher total surface charges resulting from the synergistic effect of the piezoelectric polarization and the triboelectric effect. Moreover, the peak width of the voltage output from the self-poled P(VDF-TrFE) S-TEPS (Fig. S11(a) in the ESM) is 5 times wider than the peak width of the voltage output from the non-poled P(VDF-TrFE) S-TEPS (Fig. S11(b) in the ESM, the voltage generated as a result of the triboelectric effect alone). The wider pulse width can be attributed to the synergistic effect of the two phenomena. However, S-TEPS with a positively polarized P(VDF-TrFE) (Fig. S7(b) in the ESM, a triboelectric negative material) and PDMS (a triboelectric negative material) exhibits a hindering effect (Fig. S12 in the ESM) with a low voltage output due to there being less of a difference between the electronegativity of the two

materials. The self-poled P(VDF-TrFE) S-TEPS detects a minimum pressure of 0.05 kPa and delivers an ultra-fast response time of <5 ms (Fig. 4(b)). Moreover, the device exhibits exceptionally high stability in both the medium- and high-pressure ranges, by sustaining a dynamic mechanical pressure of 30 kPa for 20,000 cycles and a pressure of 350 kPa for 6,000 cycles without any degradation in the performance (Figs. 4(c) and 4(d)). The conversion efficiency of the self-poled P(VDF-TrFE) S-TEPS is 5.6% (detailed calculations are provided in the supplementary material, Fig. S13 in the ESM). Figure S14 in the ESM shows a quasi-linear behavior with a nonlinearity of ±8 between the linear fit and the actual characteristics of the self-poled P(VDF-TrFE) S-TEPS. The measured output of the S-TEPS is not only determined by the applied pressure but also depends on the strain rate (Fig. S15(a) in the ESM), a distinguishing feature of all dynamic pressure sensors (including both triboelectric- and piezoelectric-based pressure sensors). The sensitivity remains almost the same during low-frequency operation, but at high frequencies, the sensitivity decreases (Figs. S15(b) and S15(c) in the ESM). High atmospheric humidity reduces the surface charges on the triboelectric material and hence affects the performance of a triboelectric device [36]. The device is fully sealed (details of the method are described in the ESM) to ensure stable performance of the device under different levels of humidity (Fig. S16 in the ESM). All the measurements taken as part of this work were performed at a high atmospheric humidity of 85% RH, such that we can say that the device operates stably even at high humidities.

### 2.3 Application of S-TEPS to smart robotics and human–machine interfaces

To demonstrate the practical applicability of the self-poled porous P(VDF-TrFE) S-TEPS, it was applied to human–machine interfaces and smart robotics. To advance the next generation of robotics, it is essential for robots to be able to detect and respond to human touch. The S-TEPS (device area = 4 cm × 2 cm) was attached to the finger of a humanoid robot (Fig. 5(a)), such that it could detect the pressure exerted by human touch. The S-TEPS generated a voltage of 3.3 and 5.3 V for gentle and hard finger contact, respectively (Fig. 5(b)). As the force of the finger contact increased, the contact area between the PDMS and P(VDF-TrFE) also increased, thus increasing the output voltage. This enables a humanoid robot to precisely

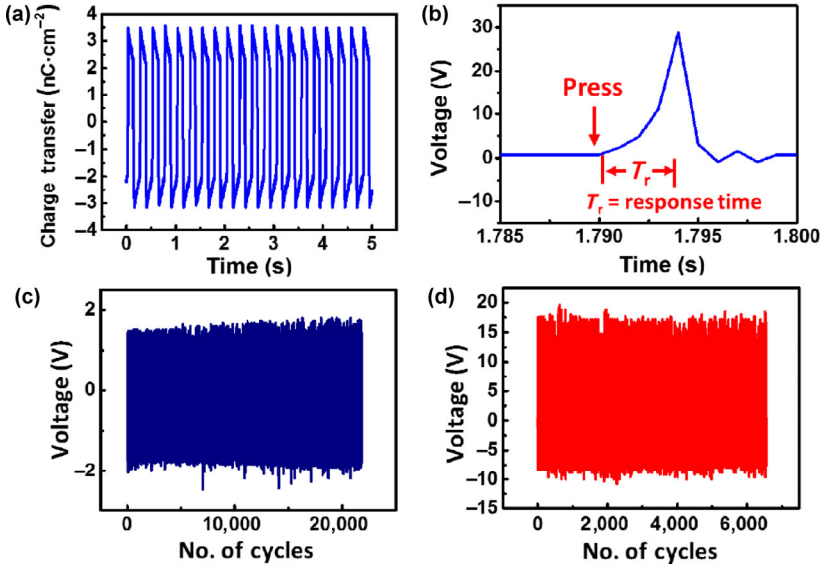


**Figure 4** (a) Charge transfer of self-poled P(VDF-TrFE) S-TEPS subjected to a pressure of 600 kPa exerted at a frequency of 5 Hz. (b) Response time of self-poled P(VDF-TrFE) S-TEPS upon application of a mechanical pressure of 600 kPa at a frequency of 5 Hz. (c) Stability of self-poled P(VDF-TrFE) S-TEPS for medium-pressure range (30 kPa). (d) Stability of self-poled P(VDF-TrFE) S-TEPS for high-pressure range (350 kPa).

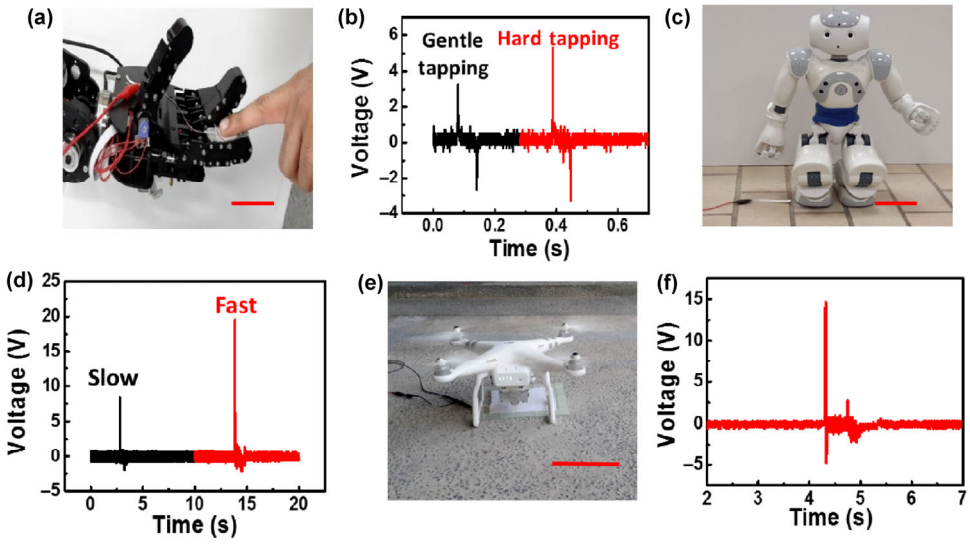


**Figure 5** Practical application of S-TEPS for human–machine interface and smart robotics. (a) S-TEPS attached to humanoid robot finger to detect pressure exerted by human touch. Scale bar: 4 cm. (b) Voltage output generated from gentle and hard finger tapping on S-TEPS attached to humanoid robot finger. (c) Photograph of S-TEPS attached to foot of humanoid robot to detect robot motion. Scale bar: 10 cm. (d) Voltage output generated during slow and fast foot tapping of humanoid robot. (e) S-TEPS application to detection of landing pressure of quadcopter robot. Scale bar: 20 cm. (f) Voltage output detected during landing of quadcopter robot.

feel and respond to human touch, thus extending the realm of the human–machine interface. To achieve a fully autonomous humanoid robot that can operate without any human intervention, it is essential for the robot to be able to self-monitor its motion. This can be achieved by attaching the S-TEPS (device area = 5 cm × 5 cm) to the foot of a humanoid robot (Fig. 5(c)). The S-TEPS generates a voltage of 8.4 and 19.6 V as a result of slow and fast foot tapping, respectively (Fig. 5(d)). As the tapping speed increases, the output voltage generated from the S-TEPS increases, thus enabling the precise identification of different speeds of humanoid motion. The fabricated S-TEPS can be effectively deployed to precisely monitor the walking speed of a humanoid robot, thus making the robot autonomous and self-sustaining.

A quadcopter robot is often used at a point distant from the location of its operator. Thus, it is essential for the operator to be able to acquire accurate information about the landing of the quadcopter. A S-TEPS (device area = 20 cm × 20 cm) was deployed to obtain information about the landing of a quadcopter by analyzing the pressure exerted by the quadcopter on a pressure sensor (Fig. 5(e)). A large quadcopter (1.2 kg) generates a voltage of 14.6 V upon landing (Fig. 5(f)), while a mini quadcopter (15.3 g) generates a voltage of 1.4 V when it lands (Fig. S17(b) in the ESM), thus demonstrating the applicability of the S-TEPS to both large and mini quadcopters. The S-TEPS was also used to detect whether the quadcopter had achieved a smooth or a crash landing, as well as detecting take-off (Fig. S17 in the ESM). In the case of a smooth landing, the S-TEPS generates a positive peak (Fig. S17(b) in the ESM, due to the contact between the P(VDF-TrFE) and PDMS), while during take-off it generates a negative peak (Fig. S17(c) in the ESM, due to the separation of the P(VDF-TrFE) and PDMS). When the quadcopter crashed-landed, the S-TEPS (Fig. S17(d) in the ESM) generated many voltage peaks due to the vibrations experienced during landing. This allows the operator (who may not be able to see the robot) to obtain accurate information about how the quadcopter robot has landed. Additionally, the S-TEPS can be used to monitor a heavy-duty industrial robotic arm (used for object manipulation) (Fig. S18 in the ESM). The S-TEPS was further used for pressure mapping (Fig. 6). A flexible pressure sensor for detecting human motion can also be fabricated (Fig. S19 in the ESM). A detailed explanation of the measurement is provided in the ESM.

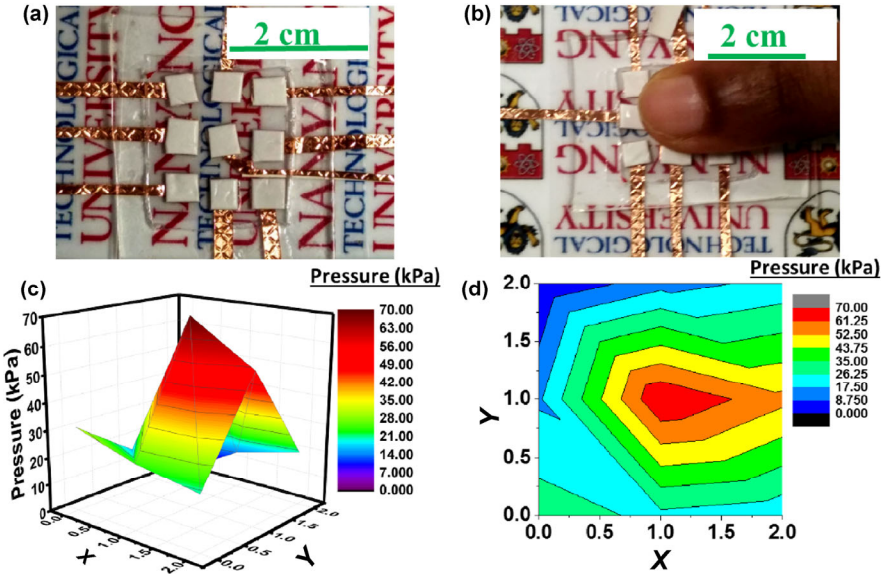


**Figure 6** (a) S-TEPS device arranged in a matrix for pressure-mapping application. (b) Application of pressure to S-TEPS by finger tapping. (c) 3D pressure map of pressure exerted on S-TEPS pressure sensor upon finger tapping. (d) 2D pressure map of pressure exerted on S-TEPS pressure sensor upon finger tapping.

## 3 Conclusion

The results presented here demonstrate that a self-polarized P(VDF-TrFE) S-TEPS can detect an ultra-large range of pressure with high sensitivity, by utilizing the synergistic effect of piezoelectric polarization and triboelectric surface charges. In this work, a novel self-poled porous P(VDF-TrFE) sponge was fabricated without the need for tedious preparatory steps such as annealing or poling. The results of this work greatly increase the scope of application for pressure sensors, by making it possible to detect a much wider range of pressures (0.05 to 600 kPa) with high sensitivity. In practice, this varies from a gentle human touch to the manipulation of heavy objects. Considering both the wide pressure-sensing range and the sensitivity, the self-polarized P(VDF-TrFE) S-TEPS exhibits the best performance amongst all the self-powered pressure sensors reported to date. This successful demonstration of a wide-range pressure sensor will enable new applications based on the precise detection of pressure (health monitoring, sensor networks, smart robotics, and sports applications), thus taking a huge step forward towards the realization of next-generation sensing devices. The strategy used in this work extends the limits of the saturation pressure for a triboelectric nanogenerator which could also be leveraged to fabricate high-power triboelectric energy harvesters.

## 4 Experimental

### 4.1 Fabrication of P(VDF-TrFE) and PDMS films

A self-poled porous P(VDF-TrFE) sponge was fabricated using the modified breath-figure technique. Polyvinyldifluoride-trifluoroethylene P(VDF-TrFE) (65 wt.%/35 wt.%, Solvay Solexis) was dissolved in N, N-dimethylformamide (DMF, Sigma-Aldrich) solvent at a polymer/solvent concentration of 70 wt.% by stirring at 70 ℃ for 4 h. The dissolved solution was subsequently drop-cast onto cleaned glass (area = 2 cm × 2 cm) and then placed on a temperature-controlled stage (Linkam Scientific Instruments) inside a humidity chamber (ETS humidity controller 5200). A temperature of −20 ℃ and a humidity of 50% RH were maintained, until a semi-solid film was formed (after approximately 1 h). The film was subsequently removed from the humidity chamber and air-dried for 6 h at room temperature until all the absorbed water was removed, leaving a porous white sponge. The sponge was peeled from the glass to produce a free-standing, flexible, self-poled P(VDF-TrFE) sponge. To understand the mechanism of self-polarization,

P(VDF-TrFE) films were fabricated at various temperatures and humidities. The temperature was varied using the temperature-controlled stage, while the humidity was varied using the humidity chamber. The thickness and area of all the P(VDF-TrFE) films fabricated under different conditions were 200 ± 10 μm and 2 cm × 2 cm, respectively. A compact P(VDF-TrFE) film (control sample) was fabricated by repeatedly spin-coating the P(VDF-TrFE) dissolved DMF solution on a glass slide (2 cm × 2 cm), until the required thickness of 200 μm was obtained.

The PDMS freestanding layer (thickness = 100 μm, area = 2 cm × 2 cm) was fabricated by curing a mixture of PDMS (Sylgard 184, Dow Corning, USA) base and curer (at a weight ratio of 10:1) at 60 °C for 2 h. The freestanding layer was obtained by peeling the PDMS layer from the substrate.

### 4.2 Fabrication of piezoelectric nanogenerator (PENG) and single-electrode triboelectric pressure sensor (S-TEPS)

To fabricate the piezoelectric nanogenerator, gold electrodes (thickness = 30 nm, area = 1 cm × 1 cm) were deposited (by sputtering) on both sides of the P(VDF-TrFE) films. The gold electrodes were connected to the measuring instruments using copper tape.

The single-electrode triboelectric pressure sensor consisted of two layers: (i) a P(VDF-TrFE) film with gold electrodes (thickness = 30 nm, area = 1 cm × 1 cm) on one side; (ii) a freestanding PDMS film. The two layers were separated by a 2-mm spacer (VHB tape). The gold electrodes were connected to one terminal of the measuring instrument, while the other terminal of the measuring instrument was connected to ground. The device was sealed by applying a thin layer of silicone rubber to the junction between the PDMS and the spacer (VHB tape). This prevents the water vapor from interacting with the triboelectric surface of the PDMS and P(VDF-TrFE), thus ensuring stable performance.

### 4.3 Characterization

The top and cross-section morphologies of the P(VDF-TrFE) films were measured using field-emission scanning electron microscopy (FESEM, JEOL 7600F). The thickness of the films was determined by a profilometer (Decktak Stylus Profilometer). The phase identifications were carried out using FTIR-ATR (PerkinElmer Frontier) and XRD (Shimadzu). The phase analysis was carried out using piezo-response force microscopy (Asylum Research). The dynamic mechanical pressure was applied by a magnetic shaker (Sinocera, Model JZK-20). The mechanical pressure was measured using one force gauge (Mark-10, Model M7-025) (for the low-pressure range) and another force gauge (Sinocera, Model CY-YD-303) (for the medium- and high-pressure ranges). The voltage outputs from the piezoelectric and triboelectric devices were measured by an oscilloscope (Trektronix, MDO 3024, input resistance = 10 MΩ). The current output was measured using a low-noise current pre-amplifier (Stanford Research System, Model SR570, input resistance = 4 Ω). The charge transfer was measured using an electrometer (Keithley 6514 system electrometer, input resistance = 200 TΩ).

## Acknowledgements

This work is supported by the National Research Foundation Investigatorship (No. NRF-NRFI2016-05) and the NRF Competitive Research Programme (No. NRF-CRP-13-2014-02). Kaushik Parida acknowledges the research scholarship provided by Nanyang Technological University, Singapore.

**Electronic Supplementary Material**: Supplementary material (voltage output and charge transfer response of the non-poled P(VDF-TrFE), schematic diagram of the negatively and positive polarized P(VDF-TrFE), voltage output of the negatively polarized P(VDF-TrFE), linearity and energy conversion efficiency of the S-TEPS, application of the S-TEPS in smart quadcopter and robotic arm) is available in the online version of this article at https://doi.org/10.1007/s12274-017-1567-6.

## References

[1] Rogers, J. A. Electronics: A diverse printed future. *Nature* **2010**, *468*, 177–178.

[2] Kim, D. H.; Lu, N. S.; Ma, R.; Kim, Y. S.; Kim, R. H.; Wang, S. D.; Wu, J.; Won, S. M.; Tao, H.; Islam, A. et al. Epidermal electronics. *Science* **2011**, *333*, 838–843.

[3] Xu, S.; Qin, Y.; Xu, C.; Wei, Y. G.; Yang, R. S.; Wang, Z. L. Self-powered nanowire devices. *Nat. Nanotechnol.* **2010**, *5*, 366–373.

[4] Tian, H.; Shu, Y.; Wang, X. F.; Mohammad, M. A.; Bie, Z.; Xie, Q. Y.; Li, C.; Mi, W. T.; Yang, Y.; Ren, T. L. A graphene-based resistive pressure sensor with record-high sensitivity in a wide pressure range. *Sci. Rep.* **2015**, *5*, 8603.

[5] Zang, Y. P.; Zhang, F. J.; Di, C. A.; Zhu, D. B. Advances of flexible pressure sensors toward artificial intelligence and health care applications. *Mater. Horiz.* **2015**, *2*, 140–156.

[6] Lipomi, D. J.; Vosgueritchian, M.; Tee, B. C. K.; Hellstrom, S. L.; Lee, J. A.; Fox, C. H.; Bao, Z. Skin-like pressure and strain sensors based on transparent elastic films of carbon nanotubes. *Nat. Nanotechnol.* **2011**, *6*, 788–792.

[7] Schwartz, G.; Tee, B. C. K.; Mei, J. G.; Appleton, A. L.; Kim, D. H.; Wang, H. L.; Bao, Z. Flexible polymer transistors with high pressure sensitivity for application in electronic skin and health monitoring. *Nat. Commun.* **2013**, *4*, 1859.

[8] Mannsfeld, S. C. B.; Tee, B. C. K.; Stoltenberg, R. M.; Chen, C. V. H. H.; Barman, S.; Muir, B. V. O.; Sokolov, A. N.; Reese, C.; Bao, Z. Highly sensitive flexible pressure sensors with microstructured rubber dielectric layers. *Nat. Mater.* **2010**, *9*, 859–864.

[9] Park, J.; Lee, Y.; Hong, J.; Ha, M.; Jung, Y. D.; Lim, H.; Kim, S. Y.; Ko, H. Giant tunneling piezoresistance of composite elastomers with interlocked microdome arrays for ultrasensitive and multimodal electronic skins. *ACS Nano* **2014**, *8*, 4689–4697.

[10] Yamada, T.; Hayamizu, Y.; Yamamoto, Y.; Yomogida, Y.; Izadi-Najafabadi, A.; Futaba, D. N.; Hata, K. A stretchable carbon nanotube strain sensor for human-motion detection. *Nat. Nanotechnol.* **2011**, *6*, 296–301.

[11] Yao, H. B.; Ge, J.; Wang, C. F.; Wang, X.; Hu, W.; Zheng, Z. J.; Ni, Y.; Yu, S. H. A flexible and highly pressure-sensitive graphene–polyurethane sponge based on fractured microstructure design. *Adv. Mater.* **2013**, *25*, 6692–6698.

[12] Lee, J. H.; Yoon, H. J.; Kim, T. Y.; Gupta, M. K.; Lee, J. H.; Seung, W.; Ryu, H.; Kim, S. W. Micropatterned P(VDF-TrFE) film-based piezoelectric nanogenerators for highly sensitive self-powered pressure sensors. *Adv. Funct. Mater.* **2015**, *25*, 3203–3209.

[13] Chun, J.; Lee, K. Y.; Kang, C. Y.; Kim, M. W.; Kim, S. W.; Baik, J. M. Embossed hollow hemisphere-based piezoelectric nanogenerator and highly responsive pressure sensor. *Adv. Funct. Mater.* **2014**, *24*, 2038–2043.

[14] Wu, W. Z.; Wen, X. N.; Wang, Z. L. Taxel-addressable matrix of vertical-nanowire piezotronic transistors for active and adaptive tactile imaging. *Science* **2013**, *340*, 952–957.

[15] Chun, J.; Kang, N. R.; Kim, J. Y.; Noh, M. S.; Kang, C. Y.; Choi, D.; Kim, S. W.; Wang, Z. L.; Baik, J. M. Highly anisotropic power generation in piezoelectric hemispheres composed stretchable composite film for self-powered motion sensor. *Nano Energy* **2015**, *11*, 1–10.

[16] Hu, Y. F.; Xu, C.; Zhang, Y.; Lin, L.; Snyder, R. L.; Wang, Z. L. A nanogenerator for energy harvesting from a rotating tire and its application as a self-powered pressure/speed sensor. *Adv. Mater.* **2011**, *23*, 4068–4071.

[17] Persano, L.; Dagdeviren, C.; Su, Y. W.; Zhang, Y. H.; Girardo, S.; Pisignano, D.; Huang, Y. G.; Rogers, J. A. High performance piezoelectric devices based on aligned arrays of nanofibers of poly(vinylidenefluoride-co-trifluoroethylene). *Nat. Commun.* **2013**, *4*, 1633.

[18] Lin, L.; Xie, Y. N.; Wang, S. H.; Wu, W. Z.; Niu, S. M.; Wen, X. N.; Wang, Z. L. Triboelectric active sensor array for self-powered static and dynamic pressure detection and tactile imaging. *ACS Nano* **2013**, *7*, 8266–8274.

[19] Fan, F.-R.; Lin, L.; Zhu, G.; Wu, W. Z.; Zhang, R.; Wang, Z. L. Transparent triboelectric nanogenerators and self-powered pressure sensors based on micropatterned plastic films. *Nano Lett.* **2012**, *12*, 3109–3114.

[20] Lee, K. Y.; Yoon, H. J.; Jiang, T.; Wen, X. N.; Seung, W.; Kim, S. W.; Wang, Z. L. Fully packaged self-powered triboelectric pressure sensor using hemispheres-array. *Adv. Energy Mater.* **2016**, *6*, 1502566.

[21] Zhu, G.; Yang, W. Q.; Zhang, T. J.; Jing, Q. S.; Chen, J.; Zhou, Y. S.; Bai, P.; Wang, Z. L. Self-powered, ultrasensitive, flexible tactile sensors based on contact electrification. *Nano Lett.* **2014**, *14*, 3208–3213.

[22] Wang, X. D.; Zhang, H. L.; Dong, L.; Han, X.; Du, W. M.; Zhai, J. Y.; Pan, C. F.; Wang, Z. L. Self-powered high-resolution and pressure-sensitive triboelectric sensor matrix for real-time tactile mapping. *Adv. Mater.* **2016**, *28*, 2896–2903.

[23] Bai, P.; Zhu, G.; Jing, Q. S.; Yang, J.; Chen, J.; Su, Y. J.; Ma, J. S.; Zhang, G.; Wang, Z. L. Membrane-based self-powered triboelectric sensors for pressure change detection and its uses in security surveillance and healthcare monitoring. *Adv. Funct. Mater.* **2014**, *24*, 5807–5813.

[24] Mandal, D.; Yoon, S.; Kim, K. J. Origin of piezoelectricity in an electrospun poly(vinylidene fluoride-trifluoroethylene) nanofiber web-based nanogenerator and nano-pressure sensor. *Macromol. Rapid Commun.* **2011**, *32*, 831–837.

[25] Sharma, T.; Je, S. S.; Gill, B.; Zhang, J. X. J. Patterning piezoelectric thin film PVDF–TrFE based pressure sensor for catheter application. *Sensor. Actuat. A: Phys.* **2012**, *177*, 87–92.

[26] Tamang, A.; Ghosh, S. K.; Garain, S.; Alam, M. M.; Haeberle, J.; Henkel, K.; Schmeisser, D.; Mandal, D. DNA-assisted β-phase nucleation and alignment of molecular dipoles in PVDF film: A realization of self-poled bioinspired flexible polymer nanogenerator for portable electronic devices. *ACS Appl. Mater. Interfaces*, **2015**, *7*, 16143–16147.

[27] Cho, Y.; Park, J. B.; Kim, B. S.; Lee, J.; Hong, W. K.; Park, I. K.; Jang, J. E.; Sohn, J. I.; Cha, S.; Kim, J. M. Enhanced energy harvesting based on surface morphology engineering of P(VDF-TrFE) film. *Nano Energy* **2015**, *16*, 524–532.

[28] Li, M. Y.; Katsouras, I.; Piliego, C.; Glasser, G.; Lieberwirth, I.; Blom, P. W. M.; de Leeuw, D. M. Controlling the microstructure of poly(vinylidene-fluoride) (PVDF) thin films for microelectronics. *J. Mater. Chem. C* **2013**, *1*, 7695–7702.

[29] García-Gutiérrez, M. C.; Linares, A.; Martín-Fabiani, I.; Hernández, J. J.; Soccio, M.; Rueda, D. R.; Ezquerra, T. A.; Reynolds, M. Understanding crystallization features of P(VDF-TrFE) copolymers under confinement to optimize ferroelectricity in nanostructures. *Nanoscale* **2013**, *5*, 6006–6012.

[30] Li, X.; Lim, Y. F.; Yao, K.; Tay, F. E. H.; Seah, K. H. P(VDF-TrFE) ferroelectric nanotube array for high energy density capacitor applications. *Phys. Chem. Chem. Phys.* **2013**, 15, 515–520.

[31] Pi, Z. Y.; Zhang, J. W.; Wen, C. Y.; Zhang, Z. B.; Wu, D. P. Flexible piezoelectric nanogenerator made of poly(vinylidenefluoride-co-trifluoroethylene) (PVDF-TrFE) thin film. *Nano Energy* **2014**, *7*, 33–41.

[32] Kusuma, D. Y.; Nguyen, C. A.; Lee, P. S. Enhanced ferroelectric switching characteristics of P(VDF-TrFE) for organic memory devices. *J. Phys. Chem. B* **2010**, *114*, 13289–13293.

[33] Whiter, R. A.; Narayan, V.; Kar-Narayan, S. A scalable nanogenerator based on self-poled piezoelectric polymer nanowires with high energy conversion efficiency. *Adv. Energy Mater.* **2014**, *4*, 1400519.

[34] Wang, X. D.; Song, J. H.; Liu, J.; Wang, Z. L. Direct-current nanogenerator driven by ultrasonic waves. *Science* **2007**, *316*, 102–105.

[35] Chang, C.; Tran, V. H.; Wang, J. B.; Fuh, Y. K.; Lin, L. W. Direct-write piezoelectric polymeric nanogenerator with high energy conversion efficiency. *Nano Lett.* **2010**, *10*, 726–731.

[36] Nguyen, V.; Zhu, R.; Yang, R. S. Environmental effects on nanogenerators. *Nano Energy* **2015**, *14*, 49–61.

[37] Parida, K.; Bhavanasi, V.; Kumar, V.; Wang, J. X.; Lee, P. S. Fast charging self-powered electric double layer capacitor. *J. Power Sources* **2017**, *342*, 70–78.

[38] Zhang, A. J.; Bai, H.; Li, L. Breath figure: A nature-inspired preparation method for ordered porous films. *Chem. Rev.* **2015**, *115*, 9801–9868.

[39] Venault, A.; Chang, Y.; Wang, D. M.; Bouyer, D. A review on polymeric membranes and hydrogels prepared by vapor-induced phase separation process. *Polym. Rev.* **2013**, *53*, 568–626.

[40] Jana, S.; Garain, S.; Sen, S.; Mandal, D. The influence of hydrogen bonding on the dielectric constant and the piezoelectric energy harvesting performance of hydrated metal salt mediated PVDF films. *Phys. Chem. Chem. Phys.* **2015**, *17*, 17429–17436.

[41] Karan, S. K.; Bera, R.; Paria, S.; Das, A. K.; Maiti, S.; Maitra, A.; Khatua, B. B. An approach to design highly durable piezoelectric nanogenerator based on self-poled PVDF/AlO-rGO flexible nanocomposite with high power density and energy conversion efficiency. *Adv. Energy Mater.* **2016**, *6*, 1601016.

[42] Chen, S. T.; Li, X.; Yao, K.; Tay, F. E. H.; Kumar, A.; Zeng, K. Y. Self-polarized ferroelectric PVDF homopolymer ultra-thin films derived from Langmuir–Blodgett deposition. *Polymer* **2012**, *53*, 1404–1408.

[43] Garain, S.; Sinha, T. K.; Adhikary, P.; Henkel, K.; Sen, S.; Ram, S.; Sinha, C.; Schmeißer, D.; Mandal, D. Self-poled transparent and flexible UV light-emitting cerium complex–PVDF composite: A high-performance nanogenerator. *ACS Appl. Mater. Interfaces* **2015**, *7*, 1298–1307.

[44] Pardo, L.; García, A.; Brebøl, K.; Piazza, D.; Galassi, C. Key issues in the characterization of porous PZT based ceramics with morphotropic phase boundary composition. *J. Electroceram.* **2007**, *19*, 413–418.

[45] Wang, Z. L.; Lin, L.; Chen, J.; Niu, S.; Zi, Y. *Triboelectric Nanogenerators*; Springer International Publishing: Switzerland, 2016.

[46] Wang, Z. L.; Chen, J.; Lin, L. Progress in triboelectric nanogenerators as a new energy technology and self-powered sensors. *Energy Environ. Sci.* **2015**, *8*, 2250–2282.

[47] Lee, K. Y.; Gupta, M. K.; Kim, S. W. Transparent flexible stretchable piezoelectric and triboelectric nanogenerators for powering portable electronics. *Nano Energy* **2015**, *14*, 139–160.

[48] Wang, Z. L. Triboelectric nanogenerators as new energy technology and self-powered sensors—Principles, problems and perspectives. *Faraday Discuss.* **2014**, *176*, 447–458.

[49] Lee, J. H.; Hinchet, R.; Kim, T. Y.; Ryu, H.; Seung, W.; Yoon, H. J.; Kim, S. W. Control of skin potential by triboelectrification with ferroelectric polymers. *Adv. Mater.* **2015**, *27*, 5553–5558.

[50] Fan, F. R.; Tang, W.; Wang, Z. L. Flexible nanogenerators for energy harvesting and self-powered electronics. *Adv. Mater.* **2016**, *28*, 4283–4305.

[51] Chun, J.; Kim, J. W.; Jung, W. S.; Kang, C. Y.; Kim, S. W.; Wang, Z. L.; Baik, J. M. Mesoporous pores impregnated with Au nanoparticles as effective dielectrics for enhancing triboelectric nanogenerator performance in harsh environments. *Energy Environ. Sci.* **2015**, *8*, 3006–3012.

[52] Wang, S. H.; Lin, L.; Wang, Z. L. Triboelectric nanogenerators as self-powered active sensors. *Nano Energy* **2015**, *11*, 436–462.

[53] Seol, M. L.; Lee, S. H.; Han, J. W.; Kim, D.; Cho, G. H.; Choi, Y. K. Impact of contact pressure on output voltage of triboelectric nanogenerator based on deformation of interfacial structures. *Nano Energy* **2015**, *17*, 63–71.

[54] Bai, P.; Zhu, G.; Zhou, Y. S.; Wang, S. H.; Ma, J. S.; Zhang, G.; Wang, Z. L. Dipole-moment-induced effect on contact electrification for triboelectric nanogenerators. *Nano Res.* **2014**, *7*, 990–997.